

A Secondary Gate As a Mechanism for Inhibition of the M2 Proton Channel by Amantadine

Myunggi Yi,[†] Timothy A. Cross,[‡] and Huan-Xiang Zhou^{*,†}

Departments of Physics and of Chemistry and Biochemistry, Institute of Molecular Biophysics, School of Computational Science, and National High Magnetic Field Laboratory, Florida State University, Tallahassee, Florida 32306

Received: January 8, 2008; Revised Manuscript Received: March 21, 2008

The mechanism of inhibition of the influenza A virus M2 proton channel by the antiviral drug amantadine has been under intense investigation. The importance of a mechanistic understanding is heightened by the prevalence of amantadine-resistant mutations. To gain mechanistic insight at the molecular level, we carried out extensive molecular dynamics simulations of the tetrameric M2 proton channel in both apo and amantadine-bound forms in a lipid bilayer. The simulation of the apo form revealed that Val27 from the four M2 subunits can form a secondary gate near the channel entrance and break the water wire in the channel pore. This gate arises from physical occlusion and the elimination of hydrogen-bonding partners for water molecules. In the presence of amantadine, the secondary gate formed by Val27 and the drug molecule lying just below form an extended blockage, which breaks the water wire throughout the simulation. The location and orientation of amantadine inside of the channel pore as found in our simulation are supported by a host of experimental observations. Our study suggests a novel role for Val27 in the inhibition of the M2 proton channel by amantadine.

The M2 protein of the influenza A virus is a tetrameric proton-selective ion channel activated by low pH, and its channel activity is essential for the life cycle of the virus. The antiviral drug amantadine inhibits the replication of the virus by putatively binding to the transmembrane domain (TMD) of the M2 proton channel.¹ However, over 90% of recent influenza A cases were found to have the S31N mutation on the M2 protein that confers amantadine resistance.² Along with experiments,^{3–9} extensive computational studies^{10–17} have been performed to model the structure of the M2 TMD and to understand the mechanisms of conductance and selectivity of the proton channel. The tetrad of H37 is part of the putative primary gate essential for channel conductance and selectivity.^{5,9} The structure of M2 TMD when amantadine is present has been determined recently by solid-state NMR spectroscopy.¹⁸ Here, we report a study aimed at modeling the binding of amantadine to M2 TMD. Our results present both mechanistic insight on the inhibition of M2 by amantadine and possible explanations for mutations leading to amantadine resistance.

We modeled an amantadine molecule into the structure of M2 TMD determined in the presence of amantadine (PDB code 2h95;¹⁸ see “Setup of Simulation Systems” and Figure S1 in Supporting Information). Amantadine was initially positioned around S31, in line with the central location of this residue in the constellation of amantadine-resistant mutations (on V27, A30, S31, and G34).³ Parallel molecular dynamics simulations

were then carried out for up to 15 ns on M2 TMD in the amantadine-bound form and in the apo form (the latter based on the apo structure found in PDB code 1nyj¹⁹).

We monitored the radii of the channel pores across M2 TMD in the apo and amantadine-bound simulations. In both simulations, the data show the existence of two blockages, one toward the channel entrance and the other toward the exit (Figure 1; Supporting Information Figure S2). The latter, peaked around $z = -10$ Å, was bordered mostly by the side chains of the four W41 residues but also those of H37, and hence, it can be identified as the primary gate. The other blockage occurred around $z = +10$ Å and was bordered by the side chains of V27 residues in the apo simulation. This “secondary” gate arose from physical occlusion by the V27 side chains; an ancillary factor may be the elimination of water molecules from this region due to the lack of hydrogen-bonding partners. In the amantadine-bound simulation, this blockage was extended by the bound amantadine toward the center of the TMD.

A water wire is an important part of the mechanism for proton conductance.²⁰ We determined whether continuous water wires were formed in our simulations by identifying hydrogen bonds between water molecules in the pores. During the apo simulation (Figure 2a–d), most of the time, the water wire was broken by both the primary and secondary gates; occasionally, it was broken by just one of them; only rarely was a continuous water wire observed. The fact that the water wire was broken by the secondary gate most of the time in the apo simulation perhaps partly explains why the opening probability of the M2 channel even when activated is very low.²¹ In the amantadine-bound

* To whom correspondence should be addressed. E-mail: zhou@sb.fsu.edu.

[†] Department of Physics, Institute of Molecular Biophysics, and School of Computational Science.

[‡] Department of Chemistry and Biochemistry and National High Magnetic Field Laboratory.

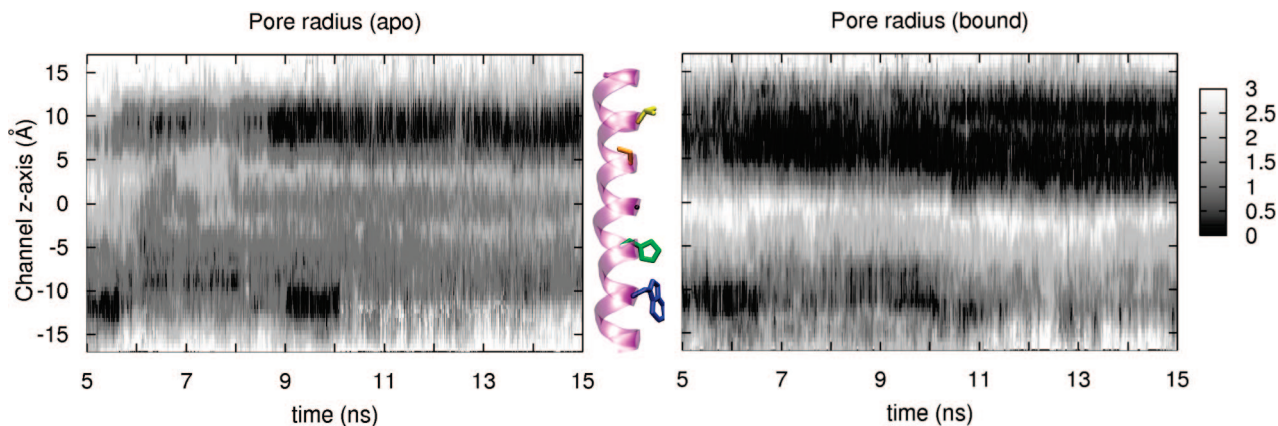


Figure 1. Pore radii of apo and amantadine-bound forms of the M2 TMD in the last 10 ns of simulations. Values of the pore radii, calculated by the HOLE program³² with a step size of 0.5 Å along the channel *z*-axis (parallel to the symmetry axis of the tetrameric TMD), are represented by a spectrum from black (0 Å) to white (≥ 3 Å). The origin of the *z*-axis was located at the center of the C $_{\alpha}$ atoms of the four G34 residues; side chains of V27 (yellow), S31 (orange), H37 (green), and W41 (blue) are shown as sticks.

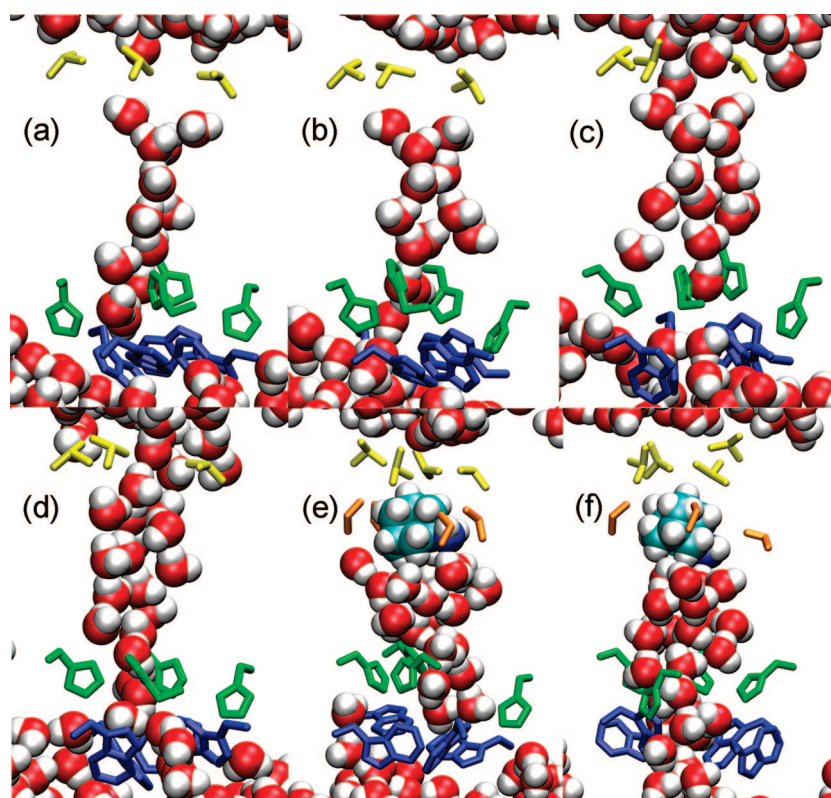


Figure 2. Representative snapshots from apo (a–d) and amantadine-bound (e–f) simulations showing breakup of water wires in the channel pores. Water and amantadine are presented as spheres (hydrogen: white; carbon: cyan; nitrogen: blue; oxygen: red); side chains of V27 (yellow), S31 (orange), H37 (green), and W41 (blue) are shown as sticks.

simulation (Figure 2e–f), the continuous blockage formed by the secondary gate and the bound amantadine always broke the water wire.

The specific interactions of amantadine with M2 TMD were analyzed by identifying contacts between the drug molecule and the channel protein. Two residues, S31 and A30, were found to contribute most to the binding site for amantadine (Supporting Information Figure S3). Three neighboring residues, V27, I33, and G34, occasionally made contacts with the bound drug molecule. In a typical snapshot (Supporting Information Figure S4; see also Figure 2e–f), the adamantane group of amantadine, with a near spherical shape, is wrapped by C $_{\beta}$ of A30 and O $_{\gamma}$ of S31 from the side and is located just below the nonpolar ring of the four V27 residues. At the bottom, the amine of

amantadine formed one or more hydrogen bonds, with partners alternating among the S31 hydroxyls, the A30 backbone carbonyls, and water molecules (amantadine made contact with at least one water molecule essentially all of the time). Thus, typically, amantadine has a downward orientation inside of M2 TMD (Supporting Information Figure S5), which is opposite to the orientation of amantadine inside a lipid bilayer.²² In a recent molecular dynamics simulation,¹⁷ amantadine binding around A29 was presented as “preliminary” results without further detail.

Neutron diffraction data of Duff et al.²³ give direct support for our observation that the binding site for amantadine is formed by S31 and A30. The same data also indicate that amantadine is oriented anisotropically and hint at a downward orientation,

as seen in our simulation. The low probability of direct contact between amantadine and V27 seen in our simulation is in line with NMR data indicating that the dipolar splitting and chemical shift of this residue are unaffected by amantadine binding.²⁴ As Figure 2e–f shows, in our simulation, amantadine is typically separated from H37 by three layers of water molecules. This separation is in contrast to a direct hydrogen bond between amantadine and H37 modeled previously²⁵ but supported by NMR data showing that the isotropic chemical shifts of H37 $N_{\delta 1}$ are unchanged upon binding amantadine.¹⁸

The binding site for amantadine found in our simulation provides rationalizations for mutational effects on the amantadine affinity of M2 TMD obtained by Astrahan et al.²⁶ They found that the A30T and S31N mutations, which confer amantadine resistance, abolish amantadine binding. Substitution by a bulkier side chain at either of these positions would reduce the volume of the putative binding site; the additional polar group would also make interactions with the nonpolar moiety of amantadine less favorable. Astrahan et al. also found that mutations of V27 (to G, A, S, or T), which too confer amantadine resistance, nevertheless retain amantadine binding. It is possible that amantadine binds to V27 mutants in a different mode. Alternatively, amantadine still binds in a similar mode, but the blockage is no longer extended by a secondary gate. We note that S31 corresponds to F in the M2 protein of influenza B virus. The substitution by a bulky side chain may significantly reduce the amantadine binding affinity,⁸ which in turn may explain the inability of amantadine to inhibit the M2 channel activity and replication of influenza B virus.²⁷

In summary, our molecular dynamics simulations suggest that the tetrad of V27 forms a secondary gate. When amantadine is bound, an extended blockage is formed, leading to breakup of the water wire and inactivation of the proton channel. Our simulation results are supported by a host of experimental observations and provide rationalizations for mutations conferring amantadine resistance. As overexpression of the M2 protein leads to a deleterious effect on intracellular protein transport²⁸ (perhaps suggesting that hyper channel activity is undesirable) and some V27 mutations are known to increase proton conductance,²⁹ it is tempting to suggest that the secondary gate formed by V27 serves an important role for attenuating the activity of the M2 proton channel.

While this paper was under review, structures of M2 TMD, determined by X-ray crystallography and solution NMR, were published.^{30,31} The X-ray structures confirm the most important features observed in our MD simulations (Supporting Information Figure S6). In particular, the channel pore “is most constricted near Val27”, providing direct support of our proposal for a secondary gate. The location and orientation of amantadine found in our simulation also agree well with those determined by X-ray crystallography. In the NMR structure, rimantadine (a close analogue of amantadine) was located in the exterior, next to residues L40, I42, and L43. Mutations of these residues did not affect amantadine binding.⁶ Such a location is favored by amantadine while it is bound to lipid bilayers.²²

Acknowledgment. This work was supported in part by NIH Grant AI023007.

Supporting Information Available: Setup of the simulation systems, details of the molecular dynamics simulations, and additional simulation results (Figures S1–S5). This material is available free of charge via the Internet at <http://pubs.acs.org>.

References and Notes

- (1) Pinto, L. H.; Lamb, R. A. *J. Biol. Chem.* **2006**, *281*, 8997.
- (2) Deyde, V. M.; Xu, X.; Bright, R. A.; Shaw, M.; Smith, C. B.; Zhang, Y.; Shu, Y.; Gubareva, L. V.; Cox, N. J.; Klimov, A. I. *J. Infect. Dis.* **2007**, *196*, 249.
- (3) Sugrue, R. J.; Hay, A. J. *Virology* **1991**, *180*, 617.
- (4) Pinto, L. H.; Holsinger, L. J.; Lamb, R. A. *Cell* **1992**, *69*, 517.
- (5) Wang, C.; Lamb, R. A.; Pinto, L. H. *Biophys. J.* **1995**, *69*, 1363.
- (6) Pinto, L. H.; Dieckmann, G. R.; Gandhi, C. S.; Papworth, C. G.; Braman, J.; Shaughnessy, M. A.; Lear, J. D.; Lamb, R. A.; DeGrado, W. F. *Proc. Natl. Acad. Sci. U.S.A.* **1997**, *94*, 11301.
- (7) Tang, Y.; Zaitseva, F.; Lamb, R. A.; Pinto, L. H. *J. Biol. Chem.* **2002**, *277*, 39880.
- (8) Stouffer, A. L.; Nanda, V.; Lear, J. D.; DeGrado, W. F. *J. Mol. Biol.* **2005**, *347*, 169.
- (9) Hu, J.; Fu, R.; Nishimura, K.; Zhang, L.; Zhou, H.-X.; Busath, D. D.; Vijayvergiya, V.; Cross, T. A. *Proc. Natl. Acad. Sci. U.S.A.* **2006**, *103*, 6865.
- (10) Sansom, M. S. P.; Kerr, I. D. *Protein Eng.* **1993**, *6*, 65.
- (11) Zhong, Q.; Husslein, T.; Moore, P. B.; Newns, D. M.; Pattnaik, P.; Klein, M. L. *FEBS Lett.* **1998**, *434*, 265.
- (12) Kukol, A.; Adams, P. D.; Rice, L. M.; Brunger, A. T.; Arkin, T. I. *J. Mol. Biol.* **1999**, *286*, 951.
- (13) Forrest, L. R.; Kukol, A.; Arkin, I. T.; Tieleman, D. P.; Sansom, M. S. *Biophys. J.* **2000**, *78*, 55.
- (14) Smondyrev, A. M.; Voth, G. A. *Biophys. J.* **2002**, *83*, 1987.
- (15) Kass, I.; Arkin, I. T. *Structure* **2005**, *13*, 1789.
- (16) Wu, Y.; Voth, G. A. *Biophys. J.* **2005**, *89*, 2402.
- (17) Chen, H.; Wu, Y.; Voth, G. A. *Biophys. J.* **2007**, *93*, 3470.
- (18) Hu, J.; Asbury, T.; Achuthan, S.; Li, C.; Bertram, R.; Quine, J. R.; Fu, R.; Cross, T. A. *Biophys. J.* **2007**, *92*, 4335.
- (19) Nishimura, K.; Kim, S.; Zhang, L.; Cross, T. A. *Biochemistry* **2002**, *41*, 13170.
- (20) Pomes, R.; Roux, B. *Biophys. J.* **1996**, *71*, 19.
- (21) Moffat, J. C.; Vijayvergiya, V.; Gao, F. P.; Cross, T. A.; Woodbury, D. J.; Busath, D. *Biophys. J.* **2008**, *94*, 434.
- (22) Li, C.; Yi, M.; Hu, J.; Zhou, H.-X.; Cross, T. A. *Biophys. J.* **2008**, *94*, 1295.
- (23) Duff, K. C.; Gilchrist, P. J.; Saxena, A. M.; Bradshaw, J. P. *Virology* **1994**, *202*, 287.
- (24) Song, Z.; Kovacs, F. A.; Wang, J.; Denny, J. K.; Shekar, S. C.; Quine, J. R.; Cross, T. A. *Biophys. J.* **2000**, *79*, 767.
- (25) Gandhi, C. S.; Shuck, K.; Lear, J. D.; Dieckmann, G. R.; DeGrado, W. F.; Lamb, R. A.; Pinto, L. H. *J. Biol. Chem.* **1999**, *274*, 5474.
- (26) Astrahan, P.; Kass, I.; Cooper, M. A.; Arkin, I. T. *Proteins* **2004**, *55*, 251.
- (27) Mould, J. A.; Paterson, R. G.; Takeda, M.; Ohigashi, Y.; Venkataraman, P.; Lamb, R. A.; Pinto, L. H. *Dev. Cell* **2003**, *5*, 175.
- (28) Sakaguchi, T.; Leser, G. P.; Lamb, R. A. *J. Cell Biol.* **1996**, *133*, 733.
- (29) Holsinger, L. J.; Nichani, D.; Pinto, L. H.; Lamb, R. A. *J. Virol.* **1994**, *68*, 1551.
- (30) Stouffer, A. L.; Acharya, R.; Salom, D.; Levine, A. S.; Di Costanzo, L.; Soto, C. S.; Tereshko, V.; Nanda, V.; Stayrook, S.; DeGrado, W. F. *Nature* **2008**, *451*, 596.
- (31) Schnell, J. R.; Chou, J. J. *Nature* **2008**, *451*, 591.
- (32) Smart, O. S.; Neduelvelil, J. G.; Wang, X.; Wallace, B. A.; Sansom, M. S. P. *J. Mol. Graphics* **1996**, *14*, 354.

JP800171M